SCATTERING OF LOW-ENERGY (5–12 eV) $C_2D_4^{\bullet+}$ IONS FROM ROOM-TEMPERATURE CARBON SURFACES

Andriy PYSANENKO[1], Jan ŽABKA[2] and Zdenek HERMAN[3,*]

V. Čermák Laboratory, J. Heyrovský Institute of Physical Chemistry, Academy of Sciences of the Czech Republic, v.v.i., Dolejškova 3, 182 23 Prague 8, Czech Republic; e-mail: [1] andriy.pysanenko@jh-inst.cas.cz, [2] jan.zabka@jh-inst.cas.cz, [3] zdenek.herman@jh-inst.cas.cz

Received April 30, 2008
Accepted June 5, 2008
Published online August 6, 2008

This paper is dedicated to Professor Rudolf Zahradník on the occasion of his 80th birthday in appreciation of his incessant activity and his many contributions to the field of theoretical chemistry.

The scattering of the hydrocarbon radical cation $C_2D_4^{\bullet+}$ from room-temperature carbon (highly oriented pyrolytic graphite, HOPG) surface was investigated at low incident energies of 6–12 eV. Mass spectra, angular and translational energy distributions of product ions were measured. From these data, information on processes at surfaces, absolute ion survival probability, and kinematics of the collision was obtained. The projectile ion showed both inelastic, dissociative and reactive scattering, namely the occurrence of H-atom transfer reaction with hydrocarbons present on the room-temperature carbon surface. The absolute survival probability of the ions for the incident angle of 30° (with respect to the surface) decreased from about 1.0% (16 eV) towards zero at incident energies below 10 eV. Estimation of the effective surface mass involved in the collision process led to $m(S)_{eff}$ of about 57 a.m.u. for inelastic non-dissociative collisions of $C_2D_4^{\bullet+}$ and of about 115 a.m.u. for fragment ions ($C_2D_3^+$, $C_2D_2^{\bullet+}$) and ions formed in reactive surface collisions ($C_2D_4H^+$, $C_2D_2H^+$, contributions to $C_2D_3^+$ and $C_2D_2^{\bullet+}$). This suggested a rather complex interaction between the projectile ion and the hydrocarbon-covered surface during the collision.

Keywords: Ion-surface scattering; Low-energy collisions; Ethylene cation; Carbon surface; Ion survival probability.

Studies of physical and chemical processes induced by impact of ions of energies below 100 eV on surfaces have found, over the last two decades, many applications ranging from surface diagnostics and surface modifications to characterization of projectile ions[1–6]. Surface-induced activation and fragmentation of projectile ions has been used as one of the methods for characterizing structural properties of polyatomic ions from relatively

doi:10.1135/cccc20080755

simple ions[2,7] to large biomolecules[8–12]. Ion-surface collisions can be an important source of information relevant to plasma–wall interactions in fusion systems[5]. This has been the main motivation for studies described in this communication. One of the important aspects of the plasma-wall interaction is information on secondary ions formed during wall erosion. Hydrocarbon ions turned out to be an important product and data on their behavior in the gas phase and in interactions with the walls of the fusion vessel are needed[13]. This includes ion survival probability, fragmentation and chemical reactions in ion-surface collisions.

In our earlier papers, we described the use of the ion-surface scattering method in obtaining information on interactions of hydrocarbon and other projectile ions with carbon surfaces[14–18]. Data on survival probability of projectile ions in collisions with room-temperature (hydrocarbon-covered) and heated (600 °C) carbon surfaces, on fragmentation processes and chemical reactions at surfaces, and on energy partitioning in surface collisions were obtained for simple hydrocarbon cations C1[14], C2 [16], cations and dications $C_7H_n^{+/2+}$ (n = 6, 7 and 8)[17], and ions from ethanol used as model polyatomic ions[15]. More recently, we reported on interactions of very low (3–10 eV) C1 hydrocarbon ions (CD_3^+, $CD_4^{\bullet+}$, and CD_5^+) with room-temperature carbon (highly oriented pyrolytic graphite, HOPG) surfaces[18]. Studies at incident energies below 15 eV brought new problems in interpreting the results associated mainly with decreasing survival probability of very slow ions in surface collisions.

In this paper, we extend our studies of surface collisions of very slow ions to the interaction of the radical cation $C_2D_4^{\bullet+}$ with room-temperature (hydrocarbon covered) HOPG surfaces. The survival probability of this ion below about 10 eV, mass spectra, angular and translational energy distributions of the product ions were determined, and the data were used to explore the kinematics of the collision.

EXPERIMENTAL

The application of the Prague beam scattering apparatus EVA II to surface studies was described earlier[6,14–18]. In the present experiments, the projectile ion $C_2D_4^{\bullet+}$ was formed by bombardment with 80 eV electrons of deuterated ethane C_2D_6 in a low-pressure ion source. The dissociative ionization of ethane leads to a more favorable internal energy distribution of the $C_2H_4^{\bullet+}$ ion[19] than direct ionization of ethene. Ions were extracted from the ionization chamber, accelerated to about 140 eV, mass-analyzed by a 90° magnet, and decelerated to the required energy in a multi-element deceleration lens. To achieve a better collimation of the low-energy projectile ion beam, an additional collimation slit (0.4 × 1 mm^2) was installed in the distance of 4 mm in front of the exit slit (0.4 × 1 mm^2) of the deceleration lens as described in the previous paper[18].

The resulting beam had an energy spread of 200 meV, full-width at half-maximum (FWHM), angular spread of 1.6°, FWHM, and geometrical dimensions of 0.4 × 1.0 mm^2 when leaving the exit slit. At ±5° the beam intensity was by a factor of 10^{-5} smaller than at its angular maximum at 0°. The collimated beam was directed towards the target carbon surface at a pre-adjusted incident angle Φ_S = 30° (measured with respect to the surface plane). Ions scattered from the surface passed through a detection slit (0.4 × 1 mm^2), located 25 mm away from the target, into a stopping potential energy analyzer. After energy analysis the ions were focused and accelerated to 1000 eV into a detection mass spectrometer (a magnetic sector instrument), and detected by counting the ions reaching a Galileo channel multiplier. The primary beam exit slit, the target, and the detection slit formed an equipotential region, carefully shielded by μ-metal sheets. The incident beam source – target section – could be rotated about the scattering center with respect to the detection slit to obtain angular distributions. Mass spectra of product ions were recorded with the stopping potential set at zero, unless stated differently. Scattering angles (Θ'_D) were measured as a deflection from the original beam direction (Θ'_D = 30° was the surface plane).

The carbon surface target was a 5 × 12 mm sample of highly oriented pyrolytic graphite (HOPG) from which the surface layer was peeled-off immediately before placing into vacuum. The sample was mounted on a stainless steel holder located 10 mm in front of the exit slit of the projectile ion deceleration system. The carbon target surfaces in the experiments were kept at room temperature. The samples could be also resistively heated up to about 1000 K and their temperature measured with a thermocouple and/or with a pyrometer. As described earlier[18], the carbon samples freshly put into vacuum were heated to 1000 K for 60 min to remove impurities and lower the fraction of ions deflected by surface charges with full incident energy. The scattering chamber of the apparatus was pumped with a 1380 l/s turbomolecular pump (Pfeiffer TMH 1600M), and the detector with a 56 l/s turbomolecular pump (Pfeiffer TMH 065); both pumps were backed by rotary vacuum pumps. The background pressure in the apparatus was about 5 × 10^{-7} torr. During the experiments the pressure was about 5 × 10^{-6} torr due to leakage of the source gas into the scattering chamber. Backstreaming of oil vapor from the rotary pump resulted, despite the installed molecular sieve trap, in covering the sample surfaces at room temperature with a layer of hydrocarbons in less than 60 min, as indicated by the occurrence of chemical reactions of H-atom transfer and C-chain build-up in experiments with radical hydrocarbon ions[14–18]. Thus in the experiments described here, the HOPG surface at room temperature was always covered with a layer of hydrocarbons (backstreaming pump oil).

The projectile ion signal to the target surface could be measured directly with an electrometer when adjusting the projectile beam. The product ions reaching the Galileo multiplier of the detection mass spectrometer were counted. For the purpose of ion survival probability determination, the count rates were transformed to ion currents.

Two corrections had to be applied to angular scattering data of the projectile ion and some of the product ions. These corrections were analyzed in detail in our previous paper[18] and became significant only for very low-energy ions of small survival probability. The first correction concerned gas-phase scattering and dissociative scattering of the incident beam by the background molecules. Its characteristics were given by the geometry of the experimental arrangement[18]. It extended below the surface plane and quickly decreased with increasing scattering angle. This correction was determined by measuring the tail of the gas-phase angular scattering without the surface sample and it concerned angular distributions of $C_2D_4^{\bullet+}$ (elastic and inelastic scattering), $C_2D_3^+$ and $C_2D_2^{\bullet+}$ (dissociative scattering).

The second correction resulted from deflection of the incident beam by local surface microcharges. Some of the low-energy projectile ions were deflected with full energy in front of the surface (unlike the inelastically scattered ions from surface collisions whose energy was substantially lower). The fraction of these deflected ions was measured by applying to the stopping potential energy analyzer a potential about 2 eV lower than the incident energy and measuring the angular distribution of the (deflected) fast projectile ion fraction. The corrections will be specified in the next section.

RESULTS AND DISCUSSION

Mass Spectra of Product Ions and Ion Survival Probability

The mass spectrum of product ions from collisions of $C_2D_4^{\bullet+}$ with room-temperature HOPG surface at the incident energy of 12.0 eV is shown in Fig. 1. The incident angle was 30° (with respect to the surface and the spectra were measured in the angular maximum at the deflection angle Θ'_D = 48° (18° with respect to the surface). The product ions were ions of *m/z* 33 ($C_2D_4H^+$ with a negligible contribution of $^{13}CCD_4^{\bullet+}$), 32 ($C_2D_4^{\bullet+}$), 30 ($C_2D_3^+$), 29 ($C_2D_2H^+$), 28 ($C_2D_2^{\bullet+}$), and 27 ($C_2DH^{\bullet+}$). To the ion signal at *m/z* 32 contributed both inelastically scattered undissociated incident ions and incident ions deflected with full energy in front of surface by surface charges (see also later in translational energy distributions). Because of the distinctly higher energy of the latter, the peak of these fast deflected ions

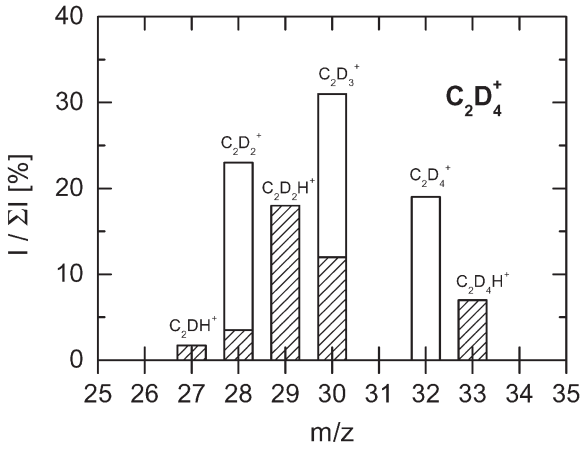

FIG. 1
Mass spectrum of product ions from collisions of $C_2D_4^{\bullet+}$ with room-temperature carbon (HOPG) surface at the incident energy 12.0 eV. Ordinate scale in % of total ion yield, $I/\Sigma I$, hatched: contributions from products of surface chemical reaction of H-atom transfer

was shifted in the mass spectrum to about *m/z* 32.25. Both direct fragmentations of the surface-excited incident ion $C_2D_4^{\bullet+}$ and fragment ions from surface chemical reaction contributed to the signal of ions at *m/z* 30 and 28. Ions of odd masses containing one hydrogen atom came from a surface chemical reaction of H-atom transfer between the projectile and hydrocarbons (H–S) on the surface (a sensitive way of detecting hydrocarbons on the surface)

$$C_2D_4^{\bullet+} + H\text{–}S \rightarrow C_2D_4H^+ (+ {}^{\bullet}S) \qquad (1)$$

and further fragmentation of the product ion formed by splitting off D_2 and D. At the same time, fragments of $C_2D_4H^+$ – formed by splitting off HD and D – gave rise to statistical contributions of chemical reaction products at *m/z* 30 and 28. The contributions of the fragmentation products from chemical reaction (*1*) are shown in Fig. 1 by hatched areas.

When the incident energy was below 10 eV, the extent of fragmentation gradually decreased. It is worth mentioning that all products of the surface chemical reaction of H-atom transfer (*m/z* 27, 29 and 33) disappeared at 6.5 eV and below this incident energy only $C_2D_4^{\bullet+}$, and a small amount of fragment ions $C_2D_3^+$ and $C_2D_2^{\bullet+}$ could be observed. Thus it appears that the H-atom transfer reaction had a threshold of about 6.5–7.0 eV.

The ion survival probability S_a (%) is defined as the percentage of intensities of all product ions ($\sum I_P$) surviving the surface collision, $S_a = 100\ \sum I_P/I_R$,

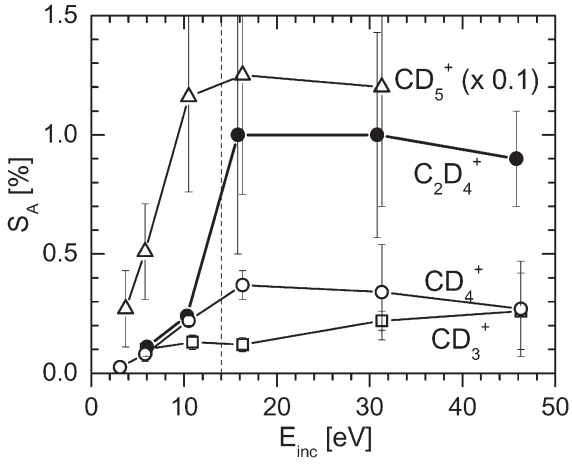

FIG. 2
Ion survival probability, S_a (in %), as a function of incident energy of hydrocarbon ions. Note a different scale for CD_5^+ (see also refs[12,14,16])

where I_R is the intensity of projectile ions incident on the target surface. The method of obtaining S_a from scattering data has been described earlier[14,16,18]. Figure 2 summarizes the data on the survival probability of small hydrocarbon ions on the incident energy of the projectile ions. Data from the present study are for $C_2D_4^{\bullet+}$ below 15 eV. Data for $C_2D_4^{\bullet+}$ at energies 15–45 eV, and for CD_3^+, $CD_4^{\bullet+}$ and CD_5^+ were reported earlier[14,16,18]. Similarly as with the C1 ions, the survival probability of $C_2D_4^{\bullet+}$ decreased to zero below 10 eV.

Angular Distributions of Product Ions

Angular distributions of product ions from interaction of $C_2D_4^{\bullet+}$ with the room-temperature HOPG surface are shown in Figs 3 and 4. The measured data (points) were subjected to a six-point smoothing procedure (thin line) and then a smooth line was drawn through the data (thicker solid line). Vertical arrows indicate scattering angles, where translational energy distributions were measured (see the next section).

Angular distributions of scattered $C_2D_4^{\bullet+}$, $C_2D_3^+$, and $C_2D_2^{\bullet+}$ had to be corrected in the vicinity of $\Theta'_D = 30°$ (surface plane) and below for a contribution of gas-phase scattering by the background gas between the exit slit of the deceleration system and the sample surface (thin solid line in Figs 3 and 4). In addition, the angular distributions of the undissociated projectile ion $C_2D_4^{\bullet+}$ had to be corrected for the contribution of the fast ions fraction which originated (ref.[18] and this section above) from deflection of very slow incident ions in front of the surface by surface charges (dashed line in Fig. 3; upper part, see also the energy peak in the translational energy distribution of $C_2D_4^{\bullet+}$ at the full incident energy of 11.25 eV in Fig. 5). Justification and application of this correction was discussed in our previous paper[18]. The pure curve of inelastic angular scattering is given by the thick solid line and its shape for $C_2D_4^{\bullet+}$ is, in view of the corrections and the scatter of experimental data, only approximate.

The final angular distributions have in general a similar shape increasing from the surface plane to peak at about 40–48° and then decreasing at larger scattering angles. The angular distributions of the pure reaction products $C_2D_4H^+$ and $C_2D_2H^+$ are very similar with a peak at 45°. The angular distributions of the fragment ions $C_2D_3^+$ and $C_2D_2^{\bullet+}$, i.e. fragment ions with contributions from both simple fragmentations of the projectile ion and fragmentations of the reaction product $C_2D_4H^+$ (Fig. 1), tend to have a broader maximum at about 40° extending to smaller scattering angles.

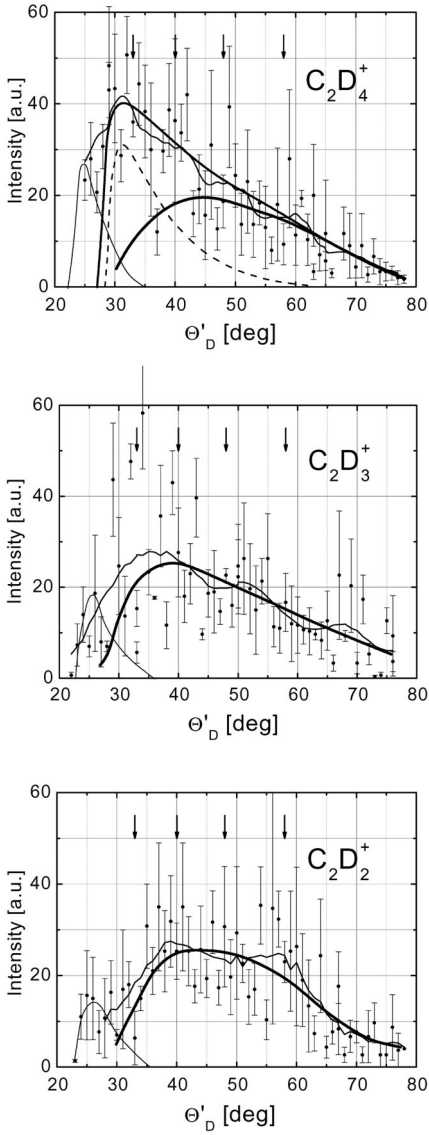

FIG. 3

Angular distributions of product ions $C_2D_4^{\bullet+}$ (upper part), $C_2D_3^+$ (middle part), and $C_2D_2^{\bullet+}$ (lower part) from collisions of $C_2D_4^{\bullet+}$ (incident energy 11.25 eV) with room-temperature HOPG. Thin line at about 30° and below – gas-phase scattering background; dashed line in the upper part ($C_2D_4^{\bullet+}$) – fast ion contribution; thick line – net angular distribution. Vertical arrows indicate angles, where translational energy distributions were measured

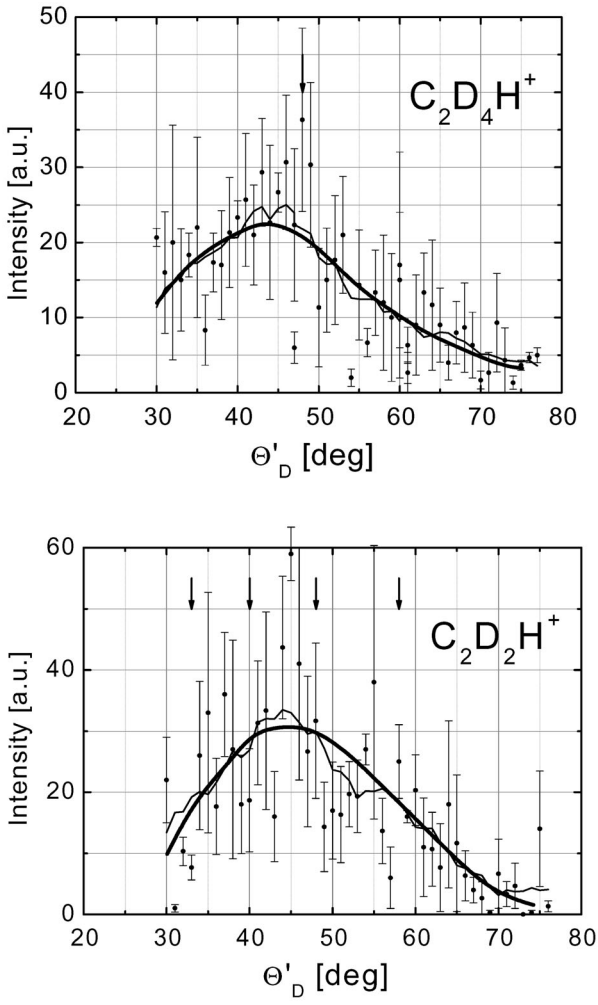

FIG. 4
Angular distributions of product ions $C_2D_4H^+$ (upper part) and $C_2D_2H^+$ (lower part) from collisions of $C_2D_4^{\bullet+}$ (11.25 eV) with room-temperature HOPG (products of reactive scattering). Vertical arrows indicate angles, where translational energy distributions were measured

Translational Energy Distributions of Product Ions

Translational energy distributions of the product ions, $P(E'_{tr})$, were measured at several scattering angles and several curves were obtained at each angle. Examples of the distributions are given in Figs 5–7. The figures show the original stopping potential data (thin solid line) and the results of 15-point smoothing (dashed line). A smooth line was then drawn through the data (thicker solid line) and the final translational energy distributions, $P(E'_{tr})$, were obtained as its derivative (solid line). The surface collisions were inelastic and the energy of product ions was substantially smaller than

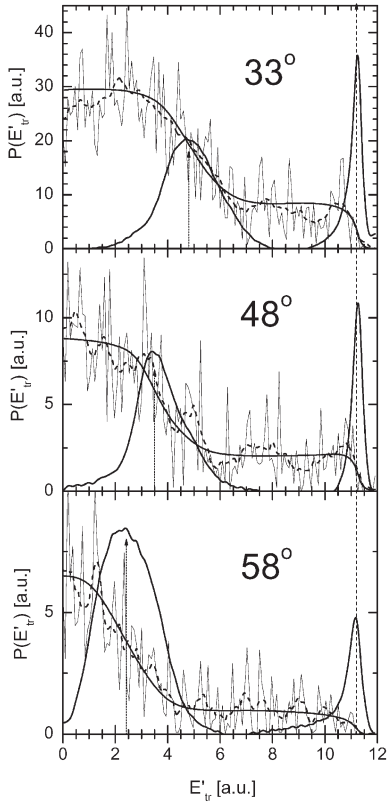

FIG. 5
Translational energy distributions, $P(E'_{tr})$, of product ions $C_2D_4^{\bullet+}$ from collisions of $C_2D_4^{\bullet+}$ (11.25 eV) with room-temperature HOPG at three different scattering angles. The peak at 11.25 eV corresponds to projectile ions of full incident energy deflected by surface charges

the incident energy (11.25 eV). The position of the peaks depended on the scattering angle.

Translational energy distributions of $C_2D_4^{\bullet+}$ (Fig. 5) showed both inelastic scattering of the undissociated projectile ion with a peak the position of which decreases with increasing angle from 4.8 eV (33°) to 2.4 eV (58°). The distributions then showed a narrow peak at 11.25 eV (incident projectile energy). This peak resulted from projectile ions deflected with full energy by surface charges in front of the surface (see previous section and ref.[18]).

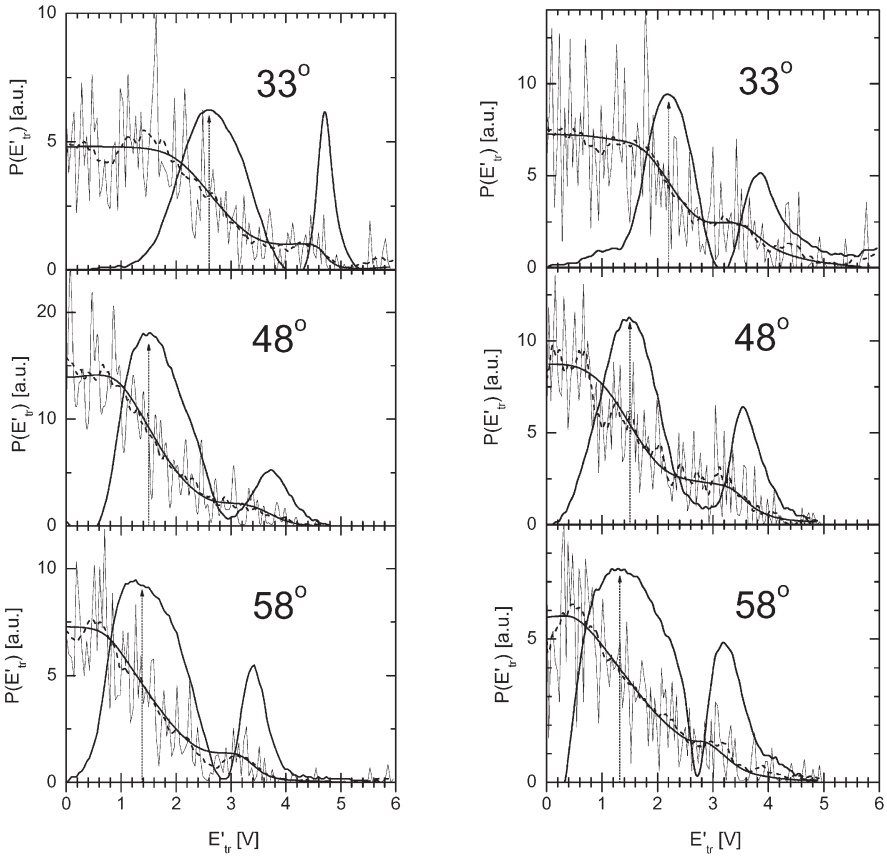

FIG. 6
Translational energy distributions, $P(E'_{tr})$, of product ions $C_2D_3^+$ (left) and $C_2D_2^{\bullet+}$ (right) from collisions of $C_2D_4^{\bullet+}$ (11.25 eV) with room-temperature HOPG at three different scattering angles

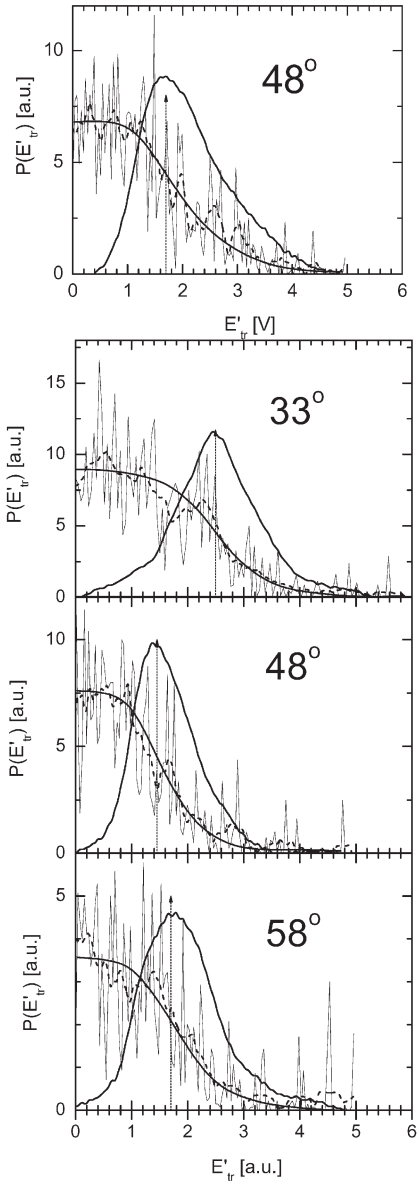

FIG. 7

Translational energy distributions, $P(E'_{tr})$, of product ions $C_2D_4H^+$ (upper part, 48°) and $C_2D_2H^+$ (lower part, scattering angles of 33, 48 and 58°) from collisions of $C_2D_4^{\bullet+}$ (11.25 eV) with room-temperature HOPG

Translational energy distributions of $C_2D_4H^+$ and $C_2D_2H^+$ peaked at substantially lower energies, between 2.4 and 1.4 eV (Fig. 7). These ions were products of surface chemical reaction (*1*) of H-atom transfer with hydrocarbons on the surface[14,16,18], $C_2D_4H^+$ being the primary product and $C_2D_2H^+$ one of the fragmentation products.

Finally, translational energy distributions of fragment ions $C_2D_3^+$ and $C_2D_2^{\bullet+}$ (Fig. 6) showed two inelastic peaks, both changing position with the scattering angle. The low-energy peaks were located at energies of 2.4 eV (2.2 eV for $C_2D_2^{\bullet+}$) and their position decreased with increasing scattering angle to about 1.4 eV. The high-energy peak occurred at 4.0–4.7 eV (33°) and with increasing scattering angle decreased to about 3.3–3.4 eV (58°). These two ions were formed both by simple fragmentation of the inelastically scattered projectile ion $C_2D_4^{\bullet+}$ and by fragmentation of the primary reaction product $C_2D_4H^+$. The high-energy peaks occurred at energies close to those in $P(E'_{tr})$ curves of $C_2D_4^{\bullet+}$, while the low-energy peaks were located in the energy region of the peaks of $P(E'_{tr})$ curves of the reaction products $C_2D_4H^+$ and $C_2D_2H^+$. Therefore, it seemed reasonable to associate the high-energy peaks with the simple fragmentation of the projectile ion and the low-energy peaks with the fragmentation of the reaction product.

Kinematic Analysis of the Scattering Data

The data on angular and translational energy distributions of product ions were used to construct a velocity scattering diagram of the ions. Analogous analyses were carried out by others for inelastic and reactive scattering in hyperthermal neutral atom – surface collisions[20,21] and by us for C1 hydrocarbon ions – carbon surface collisions[18].

A simplified kinematic analysis of the present data for $C_2D_4^{\bullet+}$ collisions with room-temperature carbon surfaces was carried out in Fig. 8. Instead of plotting the full contours, only the peaks of the velocity distributions of the product ions were plotted here[18]. The arrow on the left-hand side indicates the projectile ion incident angle (30° with respect to the surface) and $v_{inc}(C_2D_4^+)$ represents its velocity (8.25 km/s for E_{inc} = 11.25 eV) plotted from the impact point on the surface. For a surface target element fixed on the surface (v_s = 0), $v_{inc}(C_2D_4^+)$ also represents the relative velocity, v_{rel}, of the projectile of a known mass ($m(C_2D_4^+)$ = 32 a.m.u.) with respect to the target element of an effective surface mass $m(S)_{eff}$. The figure shows that the peaks of the velocity distributions of the product ions fall reasonably well on circles the centers of which bisect the relative velocity at points denoted

CM(A) (for scattered $C_2D_4^{\bullet+}$, r = 3.4 km/s) and CM(B) (for ions $C_2D_3^+$, $C_2D_2^{\bullet+}$, $C_2D_4H^+$, and $C_2D_2H^+$). From CM(B), two circles of different radii can be drawn (r_1 = 3.92 km/s and r_2 = 2.64 km/s). The respective components of the bisected relative velocity may be regarded as the center-of-mass velocities of the projectile ion, $u(C_2D_4^+)$, and the center-of-mass velocity of a surface element, u(S), of an effective surface mass $m(S)_{eff}$. From these, the effective surface mass involved in the collision may be estimated. For CM(A), one thus obtains $m_A(S)_{eff} = m(C_2D_4^+)\, u_A(C_2D_4^+)/u_A(S) = 32 \times 5.3/2.95 = 57$ a.m.u. For CM(B), one has analogously $m_B(S)_{eff} = m(C_2D_4^+)\, u_B(C_2D_4^+)/u_B(S) = 32 \times 6.45/1.8 = 115$ a.m.u.

The interpretation of the effective surface mass is by no means straightforward. It is rather unlikely that it represents the mass of the surface actually involved in the collision, though in some cases, i.e., in low-energy inelastic collisions of CD_3^+ or CD_4^+, it was found to be comparable to the mass of one or two terminal CH_3 units of surface hydrocarbons[18]. However, we believe that this parameter is of interest due to providing an insight into the complexity of the surface process. The caution in its interpretation has

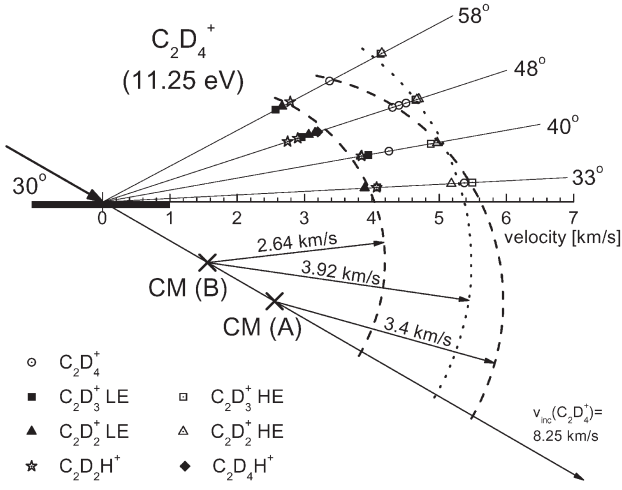

FIG. 8

A simplified scattering diagram of product ions from collisions of $C_2D_4^{\bullet+}$ (11.25 eV) with room-temperature HOPG showing peaks of velocity distributions for ions $C_2D_4^{\bullet+}$ (open points), $C_2D_3^+$ (open and full squares), $C_2D_2^{\bullet+}$ (open and full triangles), $C_2D_4H^+$ (full diamonds), $C_2D_2H^+$ (stars). For bimodal distributions, the low-velocity peaks are shown as full symbols. For details see text

several reasons. First of all, the scattering results of this type provide only average information on many collision events with a surface that is only approximately defined and may not be homogeneous. Second, drawing a circle through the inelastic scattering data assumes that energy transfer in the inelastic collision is independent of the scattering angle. This is definitely not the case in the gaseous phase, where inelastic scattering in single-collision events depends substantially on the scattering angle (see, e.g., ref.[22]). This dependence originates mostly from the change of energy transfer with the impact parameter. However, in surface scattering the scattering centers on the surface (surface atoms, terminal hydrocarbon groups) are periodically located and this may limit or minimize the influence of the impact parameter.

In our case, the effective surface mass appears slightly different for the non-dissociative inelastic scattering of the projectile ion and for fragmentation and reactive processes. For the $C_2D_4^{\bullet+}$ scattering it is formally comparable with the mass of about four terminal CH_3 groups or two terminal CH_3CH_2 groups of surface hydrocarbons, presumably indicating successive interaction with several surface centers during the time of the surface collision. For dissociative and reactive collisions the effective surface mass is about twice as large, suggesting an even more complex interaction with the surface.

The observation of a high effective surface mass is of interest in particular in the scattering of the products of H-atom transfer reaction. Many gas-phase reactions of H-atom pick-up proceed by a direct mechanism in which the projectile collides in an impulsive way with a quasi-free hydrogen atom (see, e.g., ref.[23] and references cited therein). In analogy with it, one may speculate that in the ion-surface reaction the mechanism could be similar and the average surface mass would approach the mass of the transferred H-atom. This is definitely not the case for the surface collisions of slow $C_2D_4^{\bullet+}$ described here. An analogous conclusion was reached for the system of $CD_4^{\bullet+}$ collisions with hydrocarbon-covered carbon surfaces studied earlier[18], where the effective surface mass was found to be about 48 a.m.u. A mechanism for the hydrogen transfer reaction in surface collisions was suggested earlier[24] as a rather complicated chain of processes involving projectile ion neutralization, sputtering of the proton formed in the surface, addition of the proton to the neutralized projectile, and recombination of a mobile hydrogen atom on the surface to stabilize the surface radicals formed. This chain of processes may result in a rather high apparent effective surface mass involved in the collision.

CONCLUSIONS

Collisions of the hydrocarbon radical cation $C_2D_4^{\bullet+}$ with room-temperature carbon (highly oriented pyrolytic graphite, HOPG) surface were investigated in beam-surface scattering experiments. The incident energy of the projectile ions was 6–12 eV. The data obtained consisted of mass spectra, angular and translational energy distributions of product ions. From these data, information on processes at surfaces, absolute ion survival probability, and kinematics of the collision was obtained. Inelastic, dissociative, and reactive scattering processes of the projectile ion were observed, namely the occurrence of H-atom transfer reaction with hydrocarbons present on the room-temperature carbon surface. The absolute survival probability of the ions for the incident angle of 30° (with respect to the surface) decreased from about 1.0% (16 eV) to zero at incident energies below 10 eV. Estimation of the effective surface mass involved in the collision process led to $m(S)_{eff}$ of about 57 a.m.u. for inelastic non-dissociative collisions of $C_2D_4^{\bullet+}$ and of about 115 a.m.u. for fragment ions ($C_2D_3^+$, $C_2D_2^{\bullet+}$) and ions formed in reactive surface collisions ($C_2D_4H^+$, $C_2D_2H^+$, contributions to $C_2D_3^+$ and $C_2D_2^{\bullet+}$). This suggested a rather complex interaction between the projectile ion and the surface hydrocarbons in the surface collision.

Support of this research by the Association EURATOM.IPP.CR and by the I.A.E.A. under the Research Contract No. 13488 is gratefully acknowledged.

REFERENCES

1. Rabalais J. W. (Ed.): *Low Energy Ion–Surface Interactions*. J. Wiley, New York 1994.
2. Cooks R. G., Ast T., Mabud M. D.: *Int. J. Mass Spectrom. Ion Processes* **1990**, *100*, 209.
3. Hanley L. (Ed.): *Polyatomic Ion–Surface Interactions. Int. J. Mass Spectrom. Ion Processes* **1998**, *174*, Special issue.
4. Grill V., Shen J., Evans C., Cooks R. G.: *Rev. Sci. Instrum.* **2001**, *72*, 3149.
5. Hofer W. O., Roth J. (Eds): *Physical Processes of the Interaction of Fusion Plasmas with Solids*. Academic Press, San Diego (CA) 1996.
6. Herman Z.: *J. Am. Soc. Mass Spectrom.* **2003**, *14*, 1360.
7. Wysocki V. H., Jones J. L., Ding J. M.: *J. Am. Chem. Soc.* **1991**, *113*, 8969.
8. Cooks R. G., Amy J. W., Bier M. E., Schwarz J. C., Schey K. L.: *Adv. Mass Spectrom.* **1989**, *11*, 33.
9. McCormack A. L., Jones J. L., Wysocki V. H.: *J. Am. Soc. Mass Spectrom.* **1992**, *3*, 859.
10. Rakov S., Denisov E., Laskin J., Futrell J. H.: *J. Phys. Chem. A* **2002**, *106*, 2781.
11. Meroueh O., Hase W. L.: *J. Am. Chem. Soc.* **2002**, *124*, 1524.
12. Martinez-Nunez E., Rahaman A., Hase W. L.: *J. Phys. Chem. C* **2007**, *111*, 354.
13. Philipps V., Roth J., Loarte A.: *Conclusions of the Conference of the Task Force "Plasma–Wall Interactions". Cadarache, CEA, October 17–19, 2005*.

14. Roithová J., Žabka J., Dolejšek Z., Herman Z.: *J. Phys. Chem. B* **2002**, *106*, 8293.
15. Žabka J., Dolejšek Z., Roithová J., Grill V., Märk T. D., Herman Z.: *Int. J. Mass Spectrom.* **2002**, *213*, 145.
16. Jašík J., Žabka J., Feketeová L., Ipolyi I., Märk T. D., Herman Z.: *J. Phys. Chem. A* **2005**, *109*, 10208.
17. Jašík J., Roithová J., Žabka J., Pysanenko A., Feketeová L., Ipolyi I., Märk T. D., Herman Z.: *Int. J. Mass Spectrom.* **2006**, *249–250*, 162.
18. Pysanenko A., Žabka J., Zappa F., Märk T. D., Herman Z.: *Int. J. Mass Spectrom.* **2008**, doi:10.1016/j.ijms.2008.02.011.
19. Qayyum A., Herman Z., Tepnual T., Mair C., Matt-Leubner S., Scheier P., Märk T. D.: *J. Phys. Chem. A* **2004**, *108*, 1.
20. Garton D. J., Minton T. K., Alagia M., Balucani N., Casavecchia P., Volpi G. G.: *J. Chem. Phys.* **2000**, *112*, 5975.
21. Zhang J., Garton D. J., Minton T. K.: *J. Chem. Phys.* **2002**, *117*, 6239.
22. Bernstein R. B. (Ed.): *Atom–Molecule Collision Theory*. Plenum Press, New York 1979.
23. Herman Z.: *Int. J. Mass Spectrom.* **2001**, *212*, 413.
24. Phelan L. M., Hayward M. J., Flynn J. C., Bernasek S. L.: *J. Phys. Chem. B* **1998**, *102*, 5667.